Title

Hepatitis C Virus Lipoviroparticles Assemble in the Endoplasmic Reticulum (ER) and Bud off from the ER to the Golgi Compartment in COPII Vesicles

Journal

Journal of Virology, 91(15)

ISSN

0022-538X

Authors

Syed, Gulam H
Khan, Mohsin
Yang, Song
et al.

Publication Date

2017-08-01

DOI

10.1128/jvi.00499-17

Peer reviewed

AMERICAN SOCIETY FOR MICROBIOLOGY | Journal of Virology®

STRUCTURE AND ASSEMBLY

Hepatitis C Virus Lipoviroparticles Assemble in the Endoplasmic Reticulum (ER) and Bud off from the ER to the Golgi Compartment in COPII Vesicles

Gulam H. Syed,* Mohsin Khan, Song Yang,* Aleem Siddiqui

Division of Infectious Diseases, University of California, San Diego, La Jolla, California, USA

ABSTRACT Hepatitis C virus (HCV) exists as a lipoprotein-virus hybrid lipoviroparticle (LVP). *In vitro* studies have demonstrated the importance of apolipoproteins in HCV secretion and infectivity, leading to the notion that HCV coopts the secretion of very-low-density lipoprotein (VLDL) for its egress. However, the mechanisms involved in virus particle assembly and egress are still elusive. The biogenesis of VLDL particles occurs in the endoplasmic reticulum (ER), followed by subsequent lipidation in the ER and Golgi compartment. The secretion of mature VLDL particles occurs through the Golgi secretory pathway. HCV virions are believed to latch onto or fuse with the nascent VLDL particle in either the ER or the Golgi compartment, resulting in the generation of LVPs. In our attempt to unravel the collaboration between HCV and VLDL secretion, we studied HCV particles budding from the ER *en route* to the Golgi compartment in COPII vesicles. Biophysical characterization of COPII vesicles fractionated on an iodixanol gradient revealed that HCV RNA is enriched in the highly buoyant COPII vesicle fractions and cofractionates with apolipoprotein B (ApoB), ApoE, and the HCV core and envelope proteins. Electron microscopy of immunogold-labeled microsections revealed that the HCV envelope and core proteins colocalize with apolipoproteins and HCV RNA in Sec31-coated COPII vesicles. Ultrastructural analysis also revealed the presence of HCV structural proteins, RNA, and apolipoproteins in the Golgi stacks. These findings support the hypothesis that HCV LVPs assemble in the ER and are transported to the Golgi compartment in COPII vesicles to embark on the Golgi secretory route.

IMPORTANCE HCV assembly and release accompany the formation of LVPs that circulate in the sera of HCV patients and are also produced in an *in vitro* culture system. The pathway of HCV morphogenesis and secretion has not been fully understood. This study investigates the exact site where the association of HCV virions with host lipoproteins occurs. Using immunoprecipitation of COPII vesicles and immunogold electron microscopy (EM), we characterize the existence of LVPs that cofractionate with lipoproteins, viral proteins, RNA, and vesicular components. Our results show that this assembly occurs in the ER, and LVPs thus formed are carried through the Golgi network by vesicular transport. This work provides a unique insight into the HCV LVP assembly process within infected cells and offers opportunities for designing antiviral therapeutic cellular targets.

KEYWORDS hepatitis C virus, LVPs, HCV maturation, VLDL, ApoB, ApoE

Received 29 March 2017 **Accepted** 12 May 2017

Accepted manuscript posted online 17 May 2017

Citation Syed GH, Khan M, Yang S, Siddiqui A. 2017. Hepatitis C virus lipoviroparticles assemble in the endoplasmic reticulum (ER) and bud off from the ER to the Golgi compartment in COPII vesicles. J Virol 91:e00499-17. https://doi.org/10.1128/JVI.00499-17.

Editor J.-H. James Ou, University of Southern California

Address correspondence to Gulam H. Syed, gulamsyed@ils.res.in, or Aleem Siddiqui, asiddiqui@ucsd.edu.

* Present address: Gulam H. Syed, Institute of Life Sciences, Bhubaneswar, Odisha, India; Song Yang, Center of Hepatology, Beijing Ditan Hospital, Capital Medical University, Beijing, China.

G.H.S. and M.K. contributed equally.

Hepatitis C virus (HCV), the common etiological agent of chronic liver disease, affects nearly 3% of the global population (1). Some infected individuals spontaneously clear the virus, but in about 80% patients, infection persists, leading to chronic hepatitis, which may progress to liver fibrosis, cirrhosis, and hepatocellular carcinoma (2). The huge costs associated with direct-acting antiviral (DAA) therapy and the

emergence of resistant mutants demand the identification of host factors crucial for supporting the HCV life cycle that can serve as potential therapeutic targets.

In the case of enveloped viruses, the cellular secretory pathway usually directs viral particles via cellular organelles, particularly the endoplasmic reticulum (ER) and the Golgi compartment (3–5). Enveloped viruses exploit the cellular secretory machinery in a way to maximize efficiency for the maturation of precursor particles and the transport of progeny particles (6–8). One of the least-understood aspects of the HCV life cycle is the process of HCV virion assembly and secretion. More efforts are required to completely understand and unravel these complex events of the HCV life cycle. The most unique feature of HCV is its existence in patient sera as an ~100-nm lipoprotein-virus hybrid particle termed the "lipoviroparticle" (LVP) (9, 10). Biochemical and biophysical characterizations of the LVP suggested that the lipoprotein component is an integral part of the infectious particle rather than a consequence of a physical association with the virus particle during circulation (11, 12). Both *in vivo* and *in vitro*, HCV exists as a heterogenous mixture of infectious and noninfectious particles and virions with a very low buoyant density (range, 1.10 to 1.14 g/ml) exhibit the highest level of infectivity (13–15). The depletion of cholesterol and triglycerides from LVPs results in a loss of infectivity (16, 17). The association with lipoproteins determines the buoyancy of the LVPs, and various components of lipoprotein particles, such as cholesterol esters, triglycerides, apolipoprotein B (ApoB), ApoE, and other exchangeable factors, such as ApoA-I and ApoCs, have been found in the LVPs of HCV-infected patients (9, 12). Some studies also confirmed a similar composition of LVPs produced *in vitro* (13, 18, 19).

Based on the requirement for very-low-density lipoprotein (VLDL) biosynthesis, ApoB, and ApoE for infectious HCV particle formation in the cell culture model, it was postulated that HCV usurps the VLDL secretory pathway for its egress (20–22). VLDL particles are synthesized in hepatocytes by a multistep process involving the cotranslational lipidation of ApoB in the ER by microsomal triglyceride transfer protein (MTP), resulting in the formation of precursor VLDL particles. Subsequent lipidation events in the ER and Golgi compartment lead to the formation of mature VLDL particles (23). The lipid-laden HCV nucleocapsids assembled on lipid droplets or lipid-rich HCV virions may fuse with nascent VLDL particles during VLDL lipidation, leading to HCV LVP morphogenesis. Recent studies favor the role of lipid mobilization from lipid droplets in the morphogenesis and secretion of HCV LVPs. The knockdown of the lipid droplet phospholipid-remodeling enzyme lysophosphatidylcholine acyltransferase 1 (LPCAT1) increases the cellular triacylglycerol content and HCV LVP secretion (24). Similarly, α/β-hydrolase domain-containing 5 (ABHD5), a lipid droplet-associated lipase, is required for the assembly and release of HCV LVPs (25). CideB, an ER- and lipid droplet (LD)-associated protein that facilitates VLDL lipidation, maturation, and trafficking, is also essential for HCV assembly (26).

However, there is considerable disagreement on the HCV secretion mechanism, with various groups making various observations. Some studies suggest that VLDL secretion is dispensable for HCV egress and favor a role of ApoE in HCV maturation and egress (22, 27, 28). It has been suggested that only ApoE is required for the production of *trans*-complemented HCV particles from nonhepatic cells and for the direct cell-to-cell transmission of HCV (29, 30). Small interfering RNA (siRNA) screens identified several components of the secretory pathway, including ER-to-Golgi transport, lipid and protein kinases involved in vesicle budding from the *trans*-Golgi network (TGN), adaptor proteins, and the recycling endosome, for HCV secretion (31). Interestingly, a recent study suggests that the egress of mature virions occurs via the TGN-endosome pathway independent of host lipoprotein secretion. Dominant negative mutants of Rab GTPases involved in TGN-endosome trafficking inhibited HCV release but did not have a concomitant effect on the secretion of ApoB or ApoE (28). While some studies favor HCV egress through the Golgi route (31–33), others suggest a noncanonical secretory pathway (34). Intriguingly, the endocytic and endosomal sorting complex required for transport (ESCRT) machineries have also been implicated in HCV secretion (35, 36). The intracellular cholesterol transport inhibitor U18666A promotes the accumulation of

HCV particles in autophagosomal and exosomal structures, reflecting the involvement of exosomes in HCV secretion (34, 37).

The vesicular transport of cargo molecules between intracellular organelles is facilitated by vesicle carriers. COPII vesicles mediate the intracellular transport of proteins and other cargo from the ER to the Golgi complex. COPII vesicles comprise an inner coat made of a Sec23/24 dimer and an outer coat consisting of a Sec13/31 heterotetramer. The guanine nucleotide exchange factor Sec12 recruits and activates the small GTPase Sar1, which in turn recruits the Sec23/Sec24 dimer. This complex then recruits the cargo and SNARE proteins. Subsequently, the recruitment of the Sec13/Sec31 heterotetramer, which self-assembles into cage-like lattice structures, drives membrane bending and vesicle budding (38). The scission of the vesicle stem results in the release of the COPII vesicles. Recent studies on collagen and VLDL secretion mechanisms demonstrate that COPII vesicle size is tightly regulated proportionate with cargo size to accommodate large cargo (39). The ER-to-Golgi transport of VLDL particles occurs in specialized COPII vesicles called VLDL transport vesicles that are larger than conventional COPII vesicles involved in secretory protein transport (41). It is likely that HCV and VLDL particles fuse or associate with VLDL during secondary lipidation events in the ER lumen, resulting in the generation of LVPs, which exit the cell through the Golgi secretory route in a fashion similar to that of VLDL.

Previous studies support the notion that HCV envelopment occurs at the ER (31). Direct evidence indicates that ectopically expressed E1 and E2 traffic through the secretory pathway in complex with lipoproteins and that the HCV envelope glycoproteins interact with the apolipoproteins in the ER (40, 50). Proceeding in this direction, in this study, we have characterized ER-to-Golgi trafficking of HCV virions to determine where HCV and VLDL secretory pathways merge, resulting in the morphogenesis of LVPs. This investigation establishes that HCV LVPs are assembled in the ER and then transported to the Golgi complex in COPII vesicles to board the Golgi secretory pathway for final egress.

RESULTS

Immunoprecipitation of intact COPII vesicles. To determine where the morphogenesis of HCV LVPs occurs, we characterized the COPII vesicles emanating from the ER in HCV-infected cells. Throughout this study, we used the highly infectious mutant strain JFH D183 of the wild-type clone JFH. JFH D183 is a chronic-phase virus that was collected at day 183 after transfection of the JFH genome during a persistent-infection experiment done to determine the coevolution of the virus and host in chronic infection (42). The JFH D183 virus harbors a G451R mutation in the E2 region responsible for rapid viral expansion kinetics, high infectious titers, and increased specific infectivity (42). The cytosol was prepared from JFH D183-infected Huh7.5.1 cells as described in Materials and Methods. The purity of the cytosolic fraction was analyzed by Western blotting to detect ER and Golgi impurities by using antibodies against ER (calnexin)- and Golgi (α-mannosidase)-specific proteins (Fig. 1A). The cytosolic fraction was devoid of both calnexin and α-mannosidase but enriched for glyceraldehyde-3-phosphate dehydrogenase (GAPDH), β-actin, and albumin, suggesting that the cytosolic fraction was not contaminated with impurities from the ER and Golgi complex (Fig. 1A). Immunoprecipitation of COPII vesicles from the cytosolic fraction was performed by using a mouse monoclonal anti-Sec31 antibody that binds specifically to the Sec31 coat protein of the outer coat of COPII vesicles. Immunoprecipitation of intact COPII vesicles was confirmed by electron microscopy (EM) analysis of COPII vesicles captured on protein G-Sepharose beads (Fig. 1B). As shown in Fig. 1B (top), we observed several vesicular structures bound to the surface of large protein G-Sepharose beads that were nearly 1 μm in diameter. At a higher magnification, several vesicles with an average diameter of nearly 60 nm bound to the surface of the large protein G-Sepharose bead are clearly visible (Fig. 1B, bottom), suggesting that immunoprecipitation with the anti-Sec31 monoclonal antibody effectively precipitated intact COPII vesicles (Fig. 1B). To further validate that immunoprecipitation successfully enriched intact COPII vesicles,

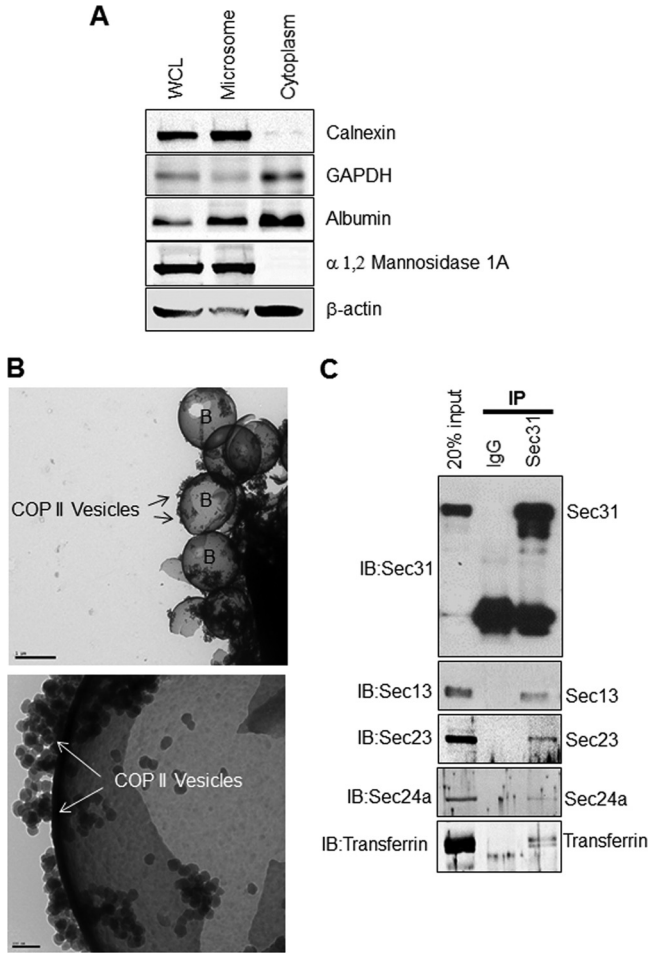

FIG 1 Immunoprecipitation of intact COPII vesicles from the cytoplasm. (A) Western blot analysis of cytoplasm purified as described in Materials and Methods. Antibodies against calnexin (ER marker) and α-1,2-mannosidase 1A (Golgi marker) were used to determine ER and Golgi contamination, respectively. WCL, whole-cell lysate. (B) The COPII vesicle–anti-Sec31 antibody immune complex bound to protein G-Sepharose was applied to regular carbon EM grids for negative-staining analysis. A representative transmission electron microscopy image shows intact COPII vesicles bound on the surface of a Sepharose bead. The top panel shows a lower-magnification image (bar, 1 μm), and the bottom panel shows a higher-magnification image (bar, 100 nm). Arrows demarcate COPII vesicles, and Sepharose beads are labeled B. (C) Western blot analysis of immunoprecipitated COP-II vesicle to determine their intactness. Sec31 and Sec13 are outer coat proteins, and Sec23 and Sec24a are inner coat proteins. Transferrin is the cargo protein. Isotype-specific IgG was used as a control. IP, immunoprecipitation; IB, immunoblotting.

we performed Western blot analysis (Fig. 1C) of the immune complexes for the COPII outer coat (Sec13 and Sec31) and inner coat (Sec23 and Sec24a) proteins and transferrin, a protein that is secreted by hepatoma cells and is a common cargo of COPII vesicles. As shown in Fig. 1C, the immune complexes with the coat protein-specific anti-Sec31 antibody were enriched for the COPII outer coat and inner coat proteins Sec31, Sec13, Sec23, Sec24, and transferrin, compared to the isotype-matched IgG control (Fig. 1C). Overall, these observations suggest that immunoprecipitation with anti-Sec31 antibody is an efficient method to precipitate intact COPII vesicles.

Mature infectious HCV particles emanate from the ER. It is widely acknowledged that HCV envelopment occurs at the ER. Furthermore, the HCV E1-E2 proteins heterodimerize on the ER membrane, further substantiating this notion (43). There is no other strong experimental evidence in this direction. To substantiate that mature infectious virus particles emanate from the ER, we evaluated the infectivity associated with COPII vesicles. We immunoprecipitated COPII vesicles and performed Western blot analysis to detect HCV structural proteins and VLDL components such as ApoE and

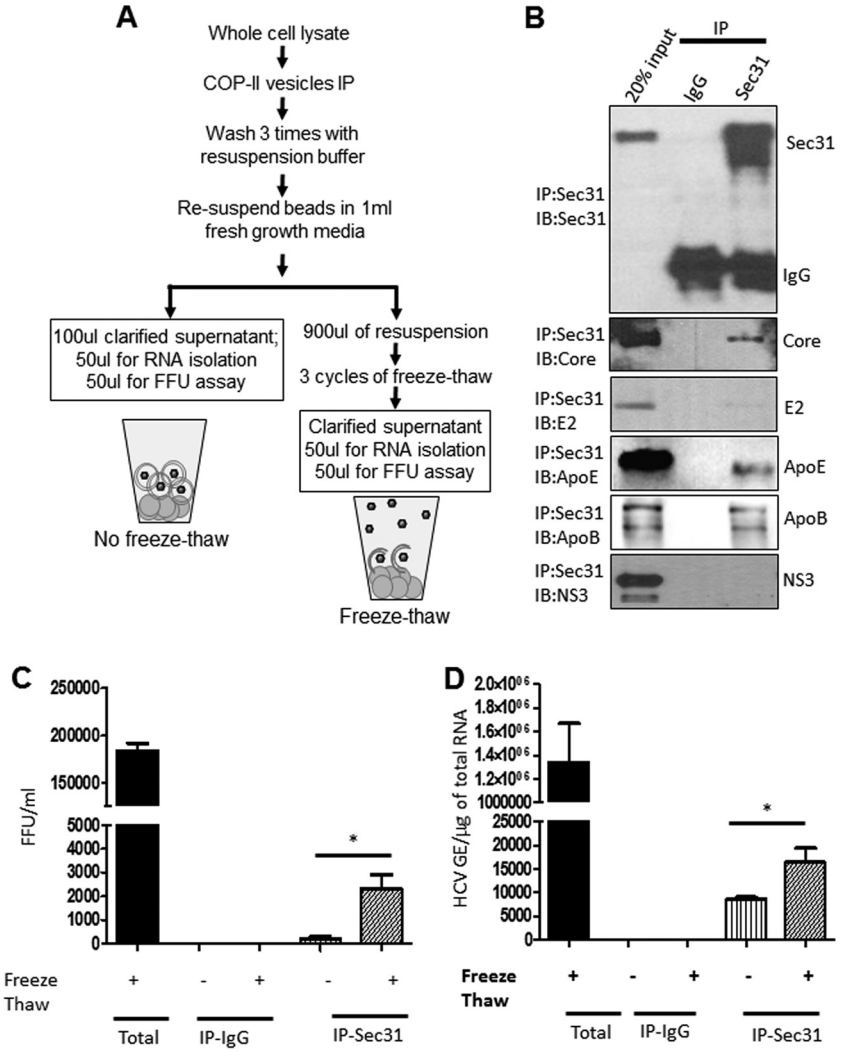

FIG 2 Mature HCV virions bud off from the ER in COPII vesicles. (A) Flow diagram depicting the experiment performed to determine the presence of infectious virions in COPII vesicles. (B) Western blot analysis of immunoprecipitated COPII vesicles to determine the presence of the HCV structural proteins E2 and core, ApoE, and ApoB. Isotype-specific IgG was used as a control. (C and D) Immunoprecipitated COPII vesicles were resuspended in cell culture medium and subjected to 4 to 5 rapid freeze-thaw cycles. The clarified supernatant was used to perform FFU assays (C), and total RNA isolated from the clarified supernatant was used to determine the presence of HCV RNA by qRT-PCR (D). Immune complexes bound to Sepharose beads not subjected to freeze-thawing were used as controls. Means ± standard deviations are shown ($n = 3$). *, $P \leq 0.05$ by an unpaired Student t test.

ApoB (Fig. 2B). Enriched COPII vesicles analyzed for the presence of the HCV nonstructural (NS) protein showed that NS3 was absent in the enriched COPII preparation (Fig. 2B). This observation ruled out the possibility of any microsomal contamination. Western blot analysis revealed that COPII vesicles carry HCV virions. Subsequently, the immunoprecipitated COPII vesicles were subjected to rapid freeze-thawing to release the virus particles harbored by COPII vesicles, as depicted in Fig. 2A. The clarified supernatant was used to perform a focus-forming unit (FFU) assay as described in Materials and Methods. Immunoprecipitations with isotype-matched IgG and COPII immune complexes not subjected to freeze-thawing were used as controls. It is evident in Fig. 2C that the COPII vesicles harbor mature infectious HCV particles. Since COPII vesicles have a very short half-life and rapidly fuse with the Golgi stacks to deliver their cargo, at a given point in time, we cannot expect higher numbers of COPII vesicles harboring infectious HCV particles. This explains the low titers associated with the COPII vesicle fractions. RNA isolated from the clarified supernatant was used to perform

quantitative reverse transcription-PCR (qRT-PCR) with HCV-specific primers to determine the level of HCV RNA associated with the COPII vesicles (Fig. 2D). The level of HCV RNA found in COPII vesicles ($\sim$1.5 $\times$ 10^4 genome equivalents [GE] per total RNA) is quite low in comparison to the level of intracellular HCV RNA found in infected cells, suggesting that only a minor fraction of COPII vesicles harbors infectious HCV virions. Lower levels of infectivity and HCV RNA were also noticed in the COPII vesicle fractions not subjected to rapid freeze-thawing and may be due to a mechanical tear of a minor fraction of the intact COPII vesicles during the experimental procedure. Notably, levels of COPII-associated HCV infectivity or RNA were found to be significantly lower than the total intracellular infectivity and HCV genome copy numbers. This observation highlights the fact that not all HCV genomic RNAs are properly assembled and successfully egress. Nonetheless, COPII vesicles carry mature infectious HCV virions (LVPs) and traffic through Golgi compartments (see below).

Characterization of COPII-mediated ER-Golgi transport of HCV LVPs. The exact site of the cross talk between the HCV and VLDL biogenesis pathways leading to the morphogenesis of HCV LVPs has not been characterized. Hence, we characterized COPII vesicular transport vesicles emanating from the ER on their way to the Golgi compartment to determine if HCV LVP morphogenesis occurs in the ER. The purified cytosol was concentrated, layered on a 6 to 30% iodixanol gradient, and subjected to ultracentrifugation at 100,000 $\times$ *g* for 6 h to fractionate the cytosolic vesicles based on their buoyancy. The rationale was to separate the COPII vesicles based on their overall size and buoyancy, envisaging that the COPII vesicles harboring HCV LVPs or VLDL particles are larger ($\sim$100 nm in diameter) and more buoyant due to the lipid-rich cargo. The resolved gradient was fractionated on a density gradient fractionator into 20 500-μl aliquots from top to bottom. Each fraction was subjected to immunoprecipitation with anti-Sec31 antibody to precipitate the COPII vesicles. The density of each fraction was determined by calculating the weight of 100 μl of each fraction (Fig. 3A, dotted line). RNA isolated from the immune complexes was subjected to qRT-PCR with HCV-specific primers to determine the presence of HCV genomes in the 20 fractions in correlation with their buoyancy (Fig. 3A). The major peak of HCV RNA was found in the first 2 buoyant fractions, followed by minor peaks in the higher-density fractions (fractions 9 to 17). The average density of the first two fractions is around 1.06 g/ml (Fig. 3A). Subsequently, we performed an elaborate Western blot analysis to determine the presence of HCV structural proteins, lipoproteins, COPII coat proteins, and traditional protein cargo of COPII vesicles, such as transferrin, in the various COPII vesicle fractions separated by buoyant density (Fig. 3B). The ER marker protein calnexin was detected to determine ER contamination of COPII vesicles. In the first two highly buoyant COPII vesicle fractions, we observed HCV RNA and envelope and core proteins, along with VLDL-specific proteins such as ApoB, ApoE, and CideB and minute amounts of COPII coat proteins such as Sec23 and Sec24 (Fig. 3B). Probably due to the lower sensitivity of the antibodies and the very minute levels of the proteins in these fractions, no effective signals were picked up for the Sec31 and Sec13 proteins in these fractions in comparison to other COPII coat proteins and associated factors such as Sec22 and CideB. Overall, these findings suggest that the buoyant COPII vesicles emanating from the ER carry mature HCV particles as either individual virions or hybrid LVPs. The COPII vesicles in subsequent denser fractions (fractions 3 to 8) contained predominantly ApoE, minor amounts of ApoB, and the HCV core and envelope proteins but lacked HCV RNA. This may be due to individual viral proteins/lipoproteins or lipoproteins in complex with HCV envelope proteins being transported in COPII vesicles. Similarly, a significant level of transferrin, which is also secreted into the extracellular milieu, is present in subsequent denser fractions 3 to 16 of COPII vesicles. The presence of low levels of HCV RNA and the HCV core and envelope proteins in the highly dense fractions (fractions 9 to 20) may be due to the presence of naked nucleocapsids and/or immature virus particles in these COPII vesicle fractions (Fig. 3B). Overall, our findings suggest that

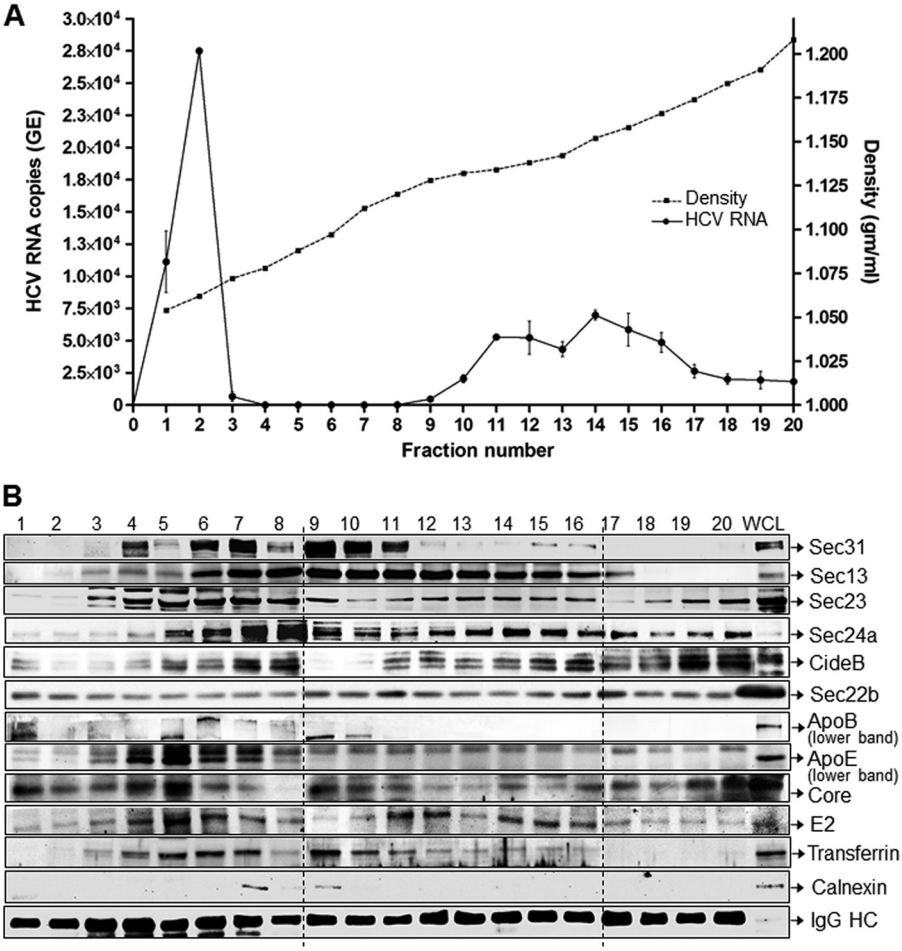

FIG 3 HCV LVP morphogenesis occurs in the ER. HCV-infected Huh7.5.1 cells were collected at 72 h postinfection and subjected to cytosol preparation as described in Materials and Methods. The concentrated cytosol was subjected to iodixanol gradient ultracentrifugation, and separated fractions 1 to 20 were used for the immunoprecipitation of COPII vesicles. (A) Total RNA isolated from immunoprecipitated COPII vesicles from each fraction was subjected to qRT-PCR for the detection of HCV RNA. The left and right axes represent HCV genome copy numbers and fraction densities, respectively. Means ± standard deviations are shown ($n = 2$). (B) Western blot analyses of immunoprecipitated COPII vesicles from each fraction were performed to detect the respective proteins as shown. The vertical dotted lines between lanes 8 and 9 and between lanes 16 and 17 demarcate the edge of each gel merged to create one single blot. WCL, whole-cell lysate (control lane); IgG HC, IgG heavy chain.

lipoprotein-associated hybrid LVPs emanate from within the ER and are transported to the Golgi compartment in COPII vesicles, similarly to VLDL particles.

Confocal and immunoelectron microscopy of HCV LVP transport vesicles. Biochemical characterization of COPII vesicles suggests that HCV and VLDL particles are present in the buoyant COPII vesicle fraction. However, it is not certain that both of these particle types are transported as hybrid particles in the same COPII vesicle. To strengthen the notion that lipoproteins coupled with the HCV components travel together as one entity in a COPII vesicle, we performed subcellular confocal imaging with various combinations of antibodies against the COPII coat protein Sec31, the viral structural proteins E2 and core, ApoE, and ApoB. These results showed that Sec31, E2, and ApoE strongly colocalize, shown as merged white spots (red [Sec31], green [E2], and blue [ApoE]) (Fig. 4A, zoomed inset). The pixel density images of total Sec31 and those representing HCV (E2)-associated ApoE and Sec31 are depicted (Fig. 4A). This quantification clearly indicates that a significant proportion of virions is associated with ApoE (Fig. 4A). Similarly, Sec31, E2, and ApoB also colocalized, represented as faint white spots due to the merging of red (Sec31), green (E2), and blue (ApoB) (Fig. 4B,

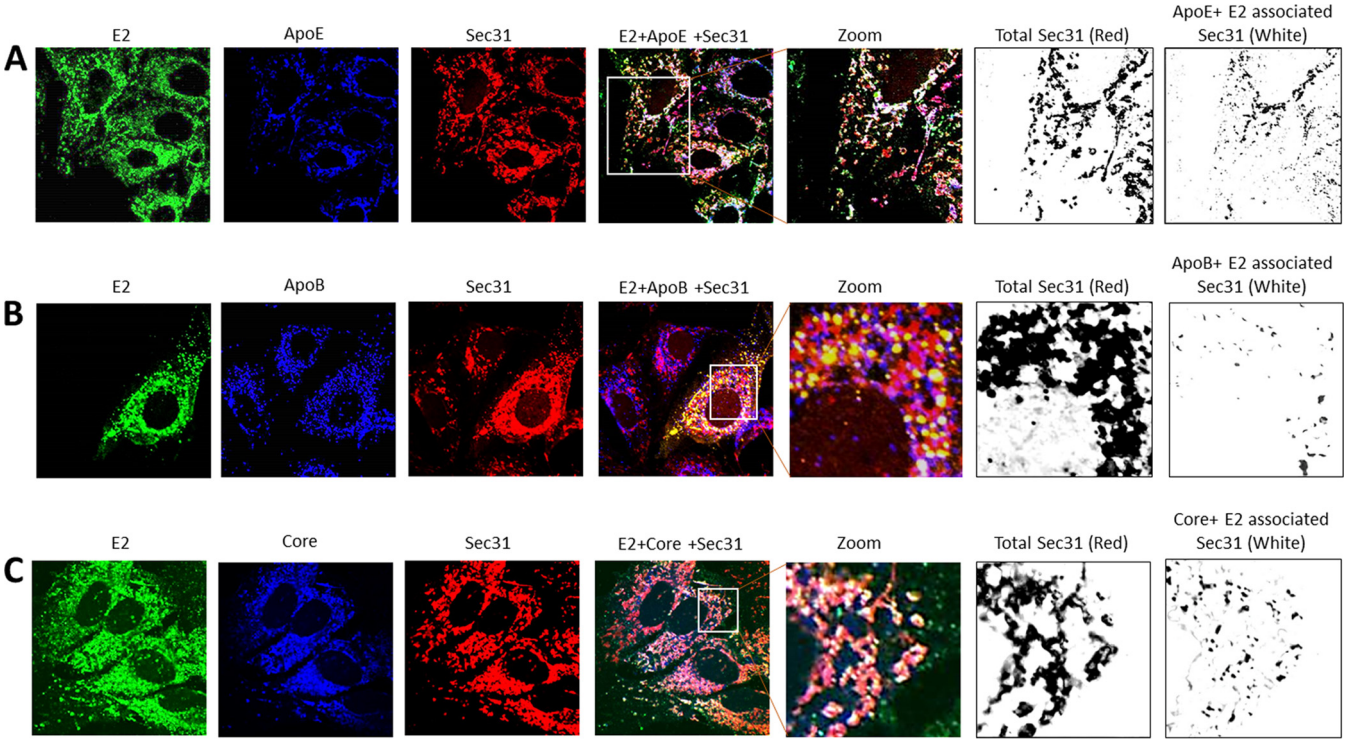

FIG 4 HCV LPVs bud from the ER in COPII vesicles. HCV-infected (MOI of 1) Huh7.5.1 cells were fixed in 4% paraformaldehyde at 72 h postinfection and subjected to immunostaining with antibodies specific for the COPII outer coat protein Sec31, HCV structural proteins, and apolipoproteins. (A) Confocal images of cells immunostained with HCV E2 (green), Sec31 (red), and ApoE (blue). The zoomed inset displays colocalization between E2, Sec31, and ApoE, seen as white spots due to the merging of green, red, and blue. Pixel density analysis of E2- and ApoE-associated COPII and total COPII (Sec31) is shown in the bottom right panel. (B) Confocal images of cells immunostained with HCV E2 (green), Sec31 (red), and ApoB (blue). The zoomed inset displays colocalization between E2, Sec31, and ApoB, seen as faint white spots due to the merging of green, red, and blue. The pixel density of E2- and ApoB-associated COPII and total COPII (Sec31) is shown in the bottom right panel. (C) Confocal images of cells immunostained with HCV E2 (green), HCV core (blue), and Sec31 (red). The zoomed inset displays colocalization between E2, core, and Sec31 as white spots due to merging of green, red, and blue. The pixel density of E2- and core-associated COPII and total COPII (Sec31) is shown in the bottom right panel.

zoomed inset). The pixel density image of HCV associated with Sec31 and ApoB is shown (Fig. 4B, far right). This pixel analysis clearly favors the association of ApoE with HCV (E2) in COPII vesicles compared to ApoB (compare far-right images in Fig. 4A and B, respectively). The colocalization of Sec31 with the HCV core and E2 proteins is also shown (Fig. 4C, zoomed inset and pixel density image). While all COPII vesicles are not associated with HCV, the overall confocal imaging results showing the colocalization of Sec31, viral structural proteins, and lipoproteins indicate that HCV LPVs may be associated with COPII vesicles (Fig. 4). However, due to the 200-nm resolution limit of conventional confocal microscopy, it is difficult to ascertain whether the viral and VLDL components colocalize within COPII vesicles with a size of nearly ~100 nm. We therefore performed immunogold electron microscopy analysis of very thin microsections of HCV-infected cells (Fig. 5). The microsections are typically 70 to 90 nm thick, and during this process, it is likely that the virus particle is also sectioned, resulting in the exposure of hidden/masked viral components such as the HCV capsid protein and genome. Huh7.5.1 cells infected with the JFH D183 virus at a multiplicity of infection (MOI) of 1 were fixed in 2% glutaraldehyde at 72 h postinfection and processed for ultracryomicrotomy. The microsections were probed with the respective primary antibodies and corresponding secondary antibodies labeled with gold particles of various sizes, as described in Materials and Methods. Immunogold EM with an antibody against Sec31 clearly shows double-membrane COPII vesicles coated with the Sec31 dimer (part of the Sec31-Sec13 heterotetramer), with each Sec31 monomer being nearly 20 nm apart (Fig. 5A). This demonstrates that immunogold EM of COPII vesicles is fairly feasible. To detect COPII vesicles and the internalized HCV LVP cargo, we stained the microsections with anti-Sec31 antibody with various combinations of antibodies spe-

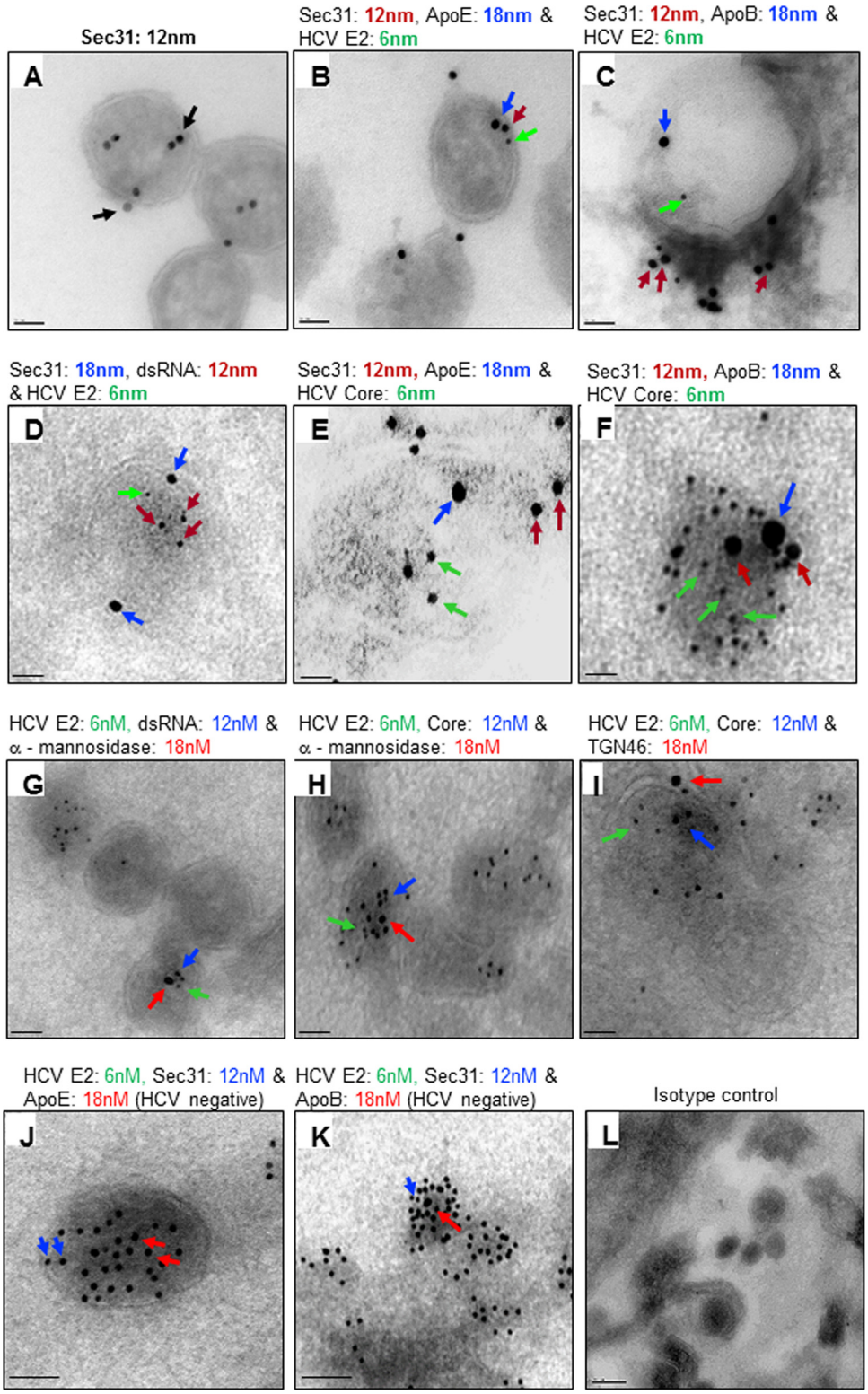

FIG 5 HCV LPVs bud from the ER in COPII vesicles. (A to I) Immunogold EM of ultrathin cryosections of HCV-infected Huh7.5.1 cells was performed to visualize the COPII vesicle content. The ultrathin cryosections were labeled with different combinations of primary antibodies against the COPII outer coat protein Sec31, HCV structural proteins, apolipoproteins, and Golgi proteins, followed by staining with the respective secondary antibodies conjugated with gold particles of 6 nm, 12 nm, and 20 nm as described in Materials and Methods. (A) Cryosections labeled for Sec31 (12 nm); (B) cryosections labeled for Sec31 (12 nm), ApoE (18 nm), and HCV E2 (6 nm); (C) cryosections labeled for Sec31 (12 nm), ApoB (18 nm), and HCV E2 (6 nm); (D) cryosections labeled for Sec31 (18 nm), dsRNA (18 nm), and HCV E2 (6 nm); (E) cryosections labeled for Sec31 (12 nm), ApoE (18 nm), and HCV core (6 nm); (F)

(Continued on next page)

cific for HCV E2, core, and RNA and VLDL components such as ApoE and ApoB. The images in Fig. 5B and C display COPII vesicles coated with Sec31 (red arrows) and harboring HCV E2 (green arrows) and ApoE (blue arrows) (B) or ApoB (blue arrows) (C). As shown in Fig. 5D, we observed a COPII vesicle harboring HCV E2 and RNA. Figures 5E to G show immunogold EM images displaying Sec31-coated COPII vesicles harboring HCV core and ApoE (Fig. 5E) or ApoB (Fig. 5F) or HCV RNA (Fig. 5G). Overall, these immunogold EM images clearly demonstrate that HCV LVPs are carried in COPII vesicles from the ER toward the Golgi compartment to embark on the Golgi secretory pathway. To demonstrate that the HCV virions traverse the Golgi secretory route during their egress, we also performed immunogold EM using antibodies against HCV components and Golgi-resident proteins such as α-mannosidase and TGN46 proteins (Fig. 5G to I). The images display the *cis*-Golgi stacks labeled with the *cis*-Golgi marker α-mannosidase, the HCV virion structural components E2 and core, and HCV RNA (the J2 antibody used here has been used widely to detect double-stranded RNA [dsRNA] intermediates of RNA viruses) (Fig. 5G and H). Similarly, the *trans*-Golgi stacks labeled with TGN46 also harbor the HCV virion structural components E2 and core (Fig. 5I). Overall, the immunogold EM images of Golgi stacks suggest that HCV particles traverse the entire route of the Golgi secretory system from the *cis*-Golgi to the *trans*-Golgi. Figures 5J to L represent uninfected cells and isotype controls, respectively. Collectively, the immuno-EM analysis clearly supports the view that COPII vesicles carry HCV LVPs to the Golgi secretory system.

Intracellular trafficking of VLDL and HCV particles. To further explore the cooperation between the intracellular trafficking of VLDL particles and HCV virions, we perturbed the intracellular trafficking of VLDL by silencing key proteins involved in ER-to-Golgi and Golgi trafficking of VLDL. Recent studies identified that CideB and Kelch-like family member 12 (KLHL12) play pivotal roles in the COPII vesicle-mediated trafficking of VLDL particles from the ER to the Golgi compartment (44, 45). Sortilin, located mainly at the TGN, functions as an intracellular sorting receptor, interacts with ApoB, and facilitates hepatic VLDL biosynthesis and release (46). We used gene-specific siRNA pools to silence the expression of CideB, sortilin, and KLHL12 in HCV-infected Huh 7.5.1 cells. Sortilin expression was almost completely knocked down, but the knockdown of CideB and KLHL12 was partial, about 50% (Fig. 6A). To characterize the significance of VLDL trafficking for HCV morphogenesis and secretion, Huh7.5.1 cells were infected with the JFH D183 virus at an MOI of 1. At 24 h postinfection, cells were transfected with gene-specific siRNA pools against CideB, sortilin, and KLHL12. HCV morphogenesis and secretion were determined at 72 h posttransfection by evaluating the intracellular and extracellular infectious titers using an FFU assay (Fig. 6B and C). Extracellular HCV RNA levels were also determined to assess the release of HCV virions into the extracellular milieu (Fig. 6D). The level of HCV replication was estimated by determining the numbers of HCV genome copies in total cellular RNA (Fig. 6E). The knockdown of CideB, sortilin, and KLHL12 significantly reduced the extracellular infectious titers of HCV (Fig. 6B). There was a corresponding increase in the intracellular infectious titers with the knockdown of CideB and KLHL12, suggesting that silencing of CideB and KLHL12 inhibits HCV secretion, resulting in the accumulation of intracellular virus (Fig. 6C). The effect of KLHL12 silencing on HCV secretion was more pronounced than that with silencing of CideB. Sortilin knockdown, however, did not result in the accumulation of intracellular virus particles (Fig. 6C), which may be due to an inhibitory effect on HCV assembly or the rapid degradation of unsecreted virus particles in

FIG 5 Legend (Continued)
cryosections labeled for Sec31 (12 nm), ApoB (18 nm), and HCV core (6 nm); (G) cryosections labeled for α-mannosidase (18 nm), dsRNA (12 nm), and HCV E2 (6 nm); (H) cryosections labeled for α-mannosidase (18 nm), HCV core (12 nm), and E2 (6 nm); (I) cryosections labeled for TGN46 (18 nm), HCV core (12 nm), and E2 (6 nm). Bars: 50 nm for panels A to D, 30 nm for panels E and F, 100 nm for panels G to I, and 50 nm for panels J to L. (J and K) Electron micrographs of uninfected controls lacking HCV E2 labeling. (L) Isotype control.

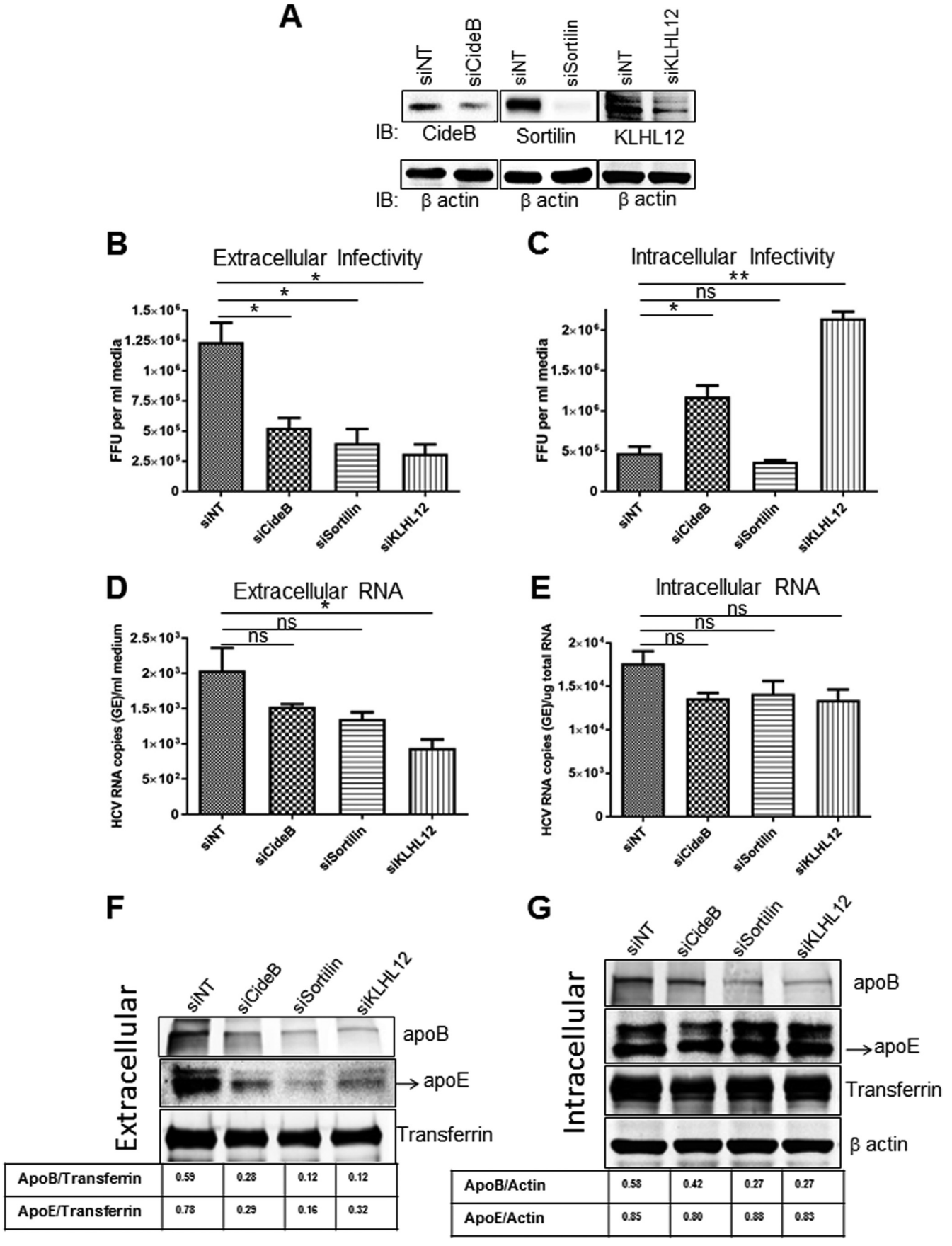
A
siNT
siCideB
siNT
siSortilin
siNT
siKLHL12
IB: CideB
Sortilin
KLHL12
IB: β actin
β actin
β actin
B
Extracellular Infectivity
FFU per ml media
siNT
siCideB
siSortilin
siKLHL12
C
Intracellular Infectivity
FFU per ml media
ns
D
Extracellular RNA
HCV RNA copies (GE)/ml medium
ns
E
Intracellular RNA
HCV RNA copies (GE)/ug total RNA
ns
F
Extracellular
apoB
apoE
Transferrin
ApoB/Transferrin 0.59 0.28 0.12 0.12
ApoE/Transferrin 0.78 0.29 0.16 0.32
G
Intracellular
apoB
apoE
Transferrin
β actin
ApoB/Actin 0.58 0.42 0.27 0.27
ApoE/Actin 0.85 0.80 0.88 0.83

sortilin-silenced cells. There was no dramatic effect of CideB, sortilin, and KLHL12 silencing on intracellular HCV RNA levels, suggesting that HCV replication is not greatly affected under these conditions (Fig. 6E). We also checked the effect of silencing of CideB, sortilin, and KLHL12 on VLDL secretion by determining the extracellular levels of ApoB and ApoE. In agreement with data from previous studies, silencing of CideB, sortilin, and KLHL12 negatively affected VLDL secretion, as determined by the extracellular levels of ApoB and ApoE in comparison to the nontargeting siRNA control (Fig. 6F). The extracellular levels of transferrin suggest that there is no effect on conventional protein cargo secretion upon silencing of CideB, sortilin, and KLHL12 (Fig. 6F). Silencing of sortilin and KLHL12 also resulted in reduced intracellular levels of ApoB (Fig. 6G), probably due to reduced ApoB expression or enhanced degradation. In summary, these results demonstrate that the perturbation of intracellular trafficking of VLDL particles negatively impacts HCV egress.

DISCUSSION

It is well established that the highly infectious virus particles found in HCV patients and in cell culture-derived HCV (HCVcc) possess buoyant density ranging from low to very low and that the association of lipoprotein components with virus particles imparts buoyancy (9–13). A recent study suggests that low levels of LVPs in patients with acute HCV infection likely results in the spontaneous clearance of acute HCV infection (47). This signifies the integral association between lipoproteins and virus particles, which promotes infectivity and prevents neutralization. Ultrastructural analyses of HCV particles derived from primary human hepatocyte cultures revealed a heterogeneous population of virus particles with a diameter ranging from 40 to 100 nm and ApoB, ApoA-I, and ApoE on the surface (18). The highly infectious purified particles have a diameter of 81 to 85 nm and display a complex internal structure (18). A proteomic analysis of cellular proteins associated with HCV virions purified by using neutralizing antibody AR3A showed that ApoE, ApoB-100, ApoA-II, ApoC-II, and ApoC-III are associated with purified HCV virions (48). Overall, these findings strongly support the notion that HCV virions are assembled and secreted as LVPs.

The current understanding about how and where the morphogenesis of the lipoprotein-virus hybrid particle occurs is incomplete. The assembly of VLDL in hepatocytes is initiated with the transfer of triglycerides to ApoB by MTP, resulting in the formation of pre-VLDL in the ER (23). The lipid-deficient pre-VLDLs undergo subsequent lipidation, resulting in mature VLDL particles (23). The ER and Golgi complex are considered to be the sites of VLDL lipidation; however, a clear understanding of these events is still lacking. Our current understanding of HCV LVP morphogenesis is that the lipid-laden HCV nucleocapsid or virion fuses with nascent VLDL particles during VLDL lipidation events in either the ER or Golgi complex, resulting in the generation of LVPs. Alternatively, immature HCV particles may mimic the VLDL precursor and undergo lipidation involving fusion with a luminal LD and the acquisition of exchangeable lipoproteins; however, this scenario does not justify the presence of ApoB in HCV LVPs (43). Dynamic imaging of HCV envelopment and secretion has not been possible due to a lack of appropriate tools. The orientation of the N-terminal ectodomains of the HCV envelope glycoproteins E1 and E2 in the ER lumen and the heterodimerization of E1-E2 on the ER membrane indirectly indicate that HCV envelopment occurs at the ER (43). A recent study indicates that HCV coopts Hrs, an ESCRT-0 component, to mediate HCV

FIG 6 HCV LVP and VLDL secretion. The effect on HCV egress was evaluated in HCV-infected Huh7.5.1 cells perturbed for VLDL secretion. (A) Western blot analysis of CideB, sortilin, and KLHL12 was performed to determine siRNA knockdown efficiency. β-Actin was used as the internal protein loading control. (B and C) At 24 h postinfection, HCV-infected Huh7.5.1 cells were transfected with nontargeting siRNA (siNT) or gene-specific siRNA pools targeting CideB (siCideB), sortilin (siSortilin), and KLHL12 (siKLHL12), and at 72 h posttransfection, the culture medium and cells were used for analyses of extracellular infectivity (B) and intracellular infectivity (C) by FFU assays. (D and E) Extracellular (D) and intracellular (E) HCV RNA levels determined by qRT-PCR (means $\pm$ standard errors of the means; $n = 3$). *, P value of $\leq$0.05; **, P value of $\leq$0.005; ns, nonsignificant (by an unpaired Student t test). (F and G) Western blot analysis of ApoB and ApoE in cell culture supernatants (F) and cell lysates (G) obtained from cells subjected to the conditions described above to judge VLDL secretion and intracellular levels of ApoB and ApoE. Transferrin was used as a control to detect levels of global protein secretion. β-Actin was used as an internal protein loading control.

envelopment, signifying the role of ESCRT proteins in the budding of HCV virions into the ER (49). The interaction of HCV envelope proteins with lipoproteins in the ER further hints at the likely morphogenesis of HCV LVPs in the ER (50). Our observations suggest that HCV envelopment occurs in the ER and strongly establish that the HCV virions budding off from the ER are enveloped and infectious (Fig. 2). A previous study conducted to elucidate the molecular determinants of HCV egress suggested that proteins involved in ER-Golgi trafficking are crucial for HCV egress (31). In agreement, an infectivity assay performed with purified COPII vesicle fractions (Fig. 2) clearly demonstrates that mature, infectious HCV particles bud off from the ER in COPII vesicles *en route* to the Golgi secretory compartment. The presence of lipoproteins in COPII vesicles isolated from buoyant cytosol fractions along with HCV structural components and genomic RNA clearly indicates that HCV LVP morphogenesis occurs in the ER (Fig. 3A and B). The presence of minor RNA peaks and HCV structural proteins in denser fractions (fractions 9 to 20) may represent the COPII-dependent secretion of individual viral proteins, immature HCV particles, and/or naked nucleocapsids (Fig. 3A and B). Highly infectious LVPs have been shown to fractionate in the buoyant fractions, having an average density of ~1.1 g/ml (10). Although it was not possible to precisely determine the density of HCV particles entrapped within COPII vesicles, most of the HCV RNA along with HCV structural proteins and lipoproteins fractionated in COPII vesicles immunoprecipitated from buoyant cytosol fractions, with densities ranging from 1.05 to 1.08 g/ml (Fig. 3A and B). The buoyancy of COPII vesicles carrying LVPs will be different from that of free LVPs; however, the high buoyancy of the COPII vesicles clearly indicates that the cargo within these vesicles is highly buoyant, resembling the LVPs. Determining the infectivity associated with the COPII vesicles immunoprecipitated from cytosol density gradient fractions was not possible due to technical issues and low virus titers due to the limited number of infectious virus particles transported in COPII vesicles at a given point in time. Overall, data from the biochemical analysis indicate that buoyant COPII vesicles transport LVPs emanating from the ER to the Golgi compartment. Confocal microscopy was performed to confirm the transport of LVPs in COPII vesicles, and although we observed a distinct colocalization between the COPII outer coat protein Sec31 and HCV structural proteins or between Sec31, HCV glycoprotein, and ApoE/ApoB (Fig. 4), due to the 200-nm resolution limit, it was difficult to ascertain the components within COPII vesicles with a size of ~100 nm. High-resolution immunogold electron microscopy confirmed that COPII vesicles transport LVPs from the ER to the Golgi compartment (Fig. 5A to E), thereby lending support to the model that HCV LVP morphogenesis happens in the ER and that LVPs are subsequently transported from the ER to the Golgi compartment in COPII vesicles.

There has been considerable debate about the route followed by HCV virions during their egress. The involvement of the Golgi secretory pathway in HCV egress, similar to the secretory route followed by VLDL particles, has been amply described (31–33). We have previously shown the role of oxysterol-binding protein (OSBP), phosphatidylinositol 4-phosphate (PI4P), and its binding partner the GOLPH3 protein, all connected with Golgi trafficking, in HCV secretion in sufficient detail (32, 33). Inhibition of HCV secretion by RNA silencing of GOLPH3 or inhibition of PI4P formation did not entirely affect VLDL secretion. We reasoned that the fraction of VLDL committed to the formation of LVPs is so minute that overall VLDL secretion may not be affected even if viral secretion is inhibited. This reasoning also applies to a recent study by Mankouri et al., in which they conclude that the inhibition of Rab GTPase did not affect VLDL secretion and therefore that VLDLs are not associated with HCV secretion (28). Some studies implicated noncanonical secretion in HCV egress involving the endosomal compartments, autophagosomes, endocytic machinery, and ESCRT proteins (35–37, 49). The presence of complex glycans on virus-associated glycoproteins substantiates that HCV virions traverse through the Golgi apparatus (43). In agreement with this view, our study indicates the transport of LVPs from the ER to the Golgi complex in COPII vesicles via the Golgi secretory route (Fig. 2, 3, and 5A to D). Further substantiating these observations, immunogold EM of the *cis*- and *trans*-Golgi stacks confirmed the presence

of HCV particles in the Golgi compartment (Fig. 5F to 5H). However, we note that the intricacies of intracellular transport have not been completely understood and involve major cross talk between the Golgi complex and endosomal and autophagy machinery. Therefore, it is plausible that HCV particles exit the Golgi secretory route and enter another secretory module prior to exiting through the plasma membrane. While the role of the exchangeable apolipoprotein ApoE in HCV maturation and postenvelopment processing is widely accepted (51), there is considerable disagreement over the role of ApoB in HCV maturation and egress. The interaction of the HCV envelope glycoproteins E1 and E2 with ApoB and ApoE at the ER hints that the glycoprotein-apolipoprotein complex could initiate the formation of hybrid lipoviroparticles (50). The presence of ApoB, along with other exchangeable apolipoproteins such as ApoE, ApoA-II, ApoC-II, and ApoC-III, on HCV virions emphasizes its role in HCV maturation and egress (18, 48). In correlation, immunogold electron microscopy clearly indicated the presence of ApoB, although in small amounts, and ApoE along with the HCV structural proteins in COPII vesicles, suggesting that the viral particles that bud from the ER are associated with ApoB and ApoE (Fig. 5B, C, E, and F), as was also previously noted on HCV virions (18). To verify that HCV coopts VLDL secretion for its egress, we targeted VLDL transport from the ER to the Golgi complex and through the Golgi complex by silencing CideB, KLHL12, and sortilin (44–46). Although VLDL secretion, as judged by the extracellular levels of ApoB and ApoE (Fig. 6F), was dramatically affected by the silencing of CideB, KLHL12, and sortilin, the effect on HCV egress was significant but moderate (Fig. 6B and D). We observed a concomitant increase in intracellular virus titers with the silencing of CideB and KLHL12, which is suggestive of an inhibition of virion secretion. However, sortilin silencing affected both the extracellular and intracellular virus titers, suggesting that it is involved in both HCV maturation and egress (Fig. 6B and C). Several reports suggest a complex role for sortilin in hepatic lipid metabolism (52), which may explain the effect of sortilin on both HCV egress and morphogenesis. Only a limited proportion of the VLDL secretory machinery may drive HCV egress, justifying the moderate effect on HCV egress due to perturbed VLDL secretion (Fig. 6). Alternatively, after morphogenesis, LVPs may be secreted completely independent of VLDL secretion. In summary, this study clearly establishes that LVP morphogenesis occurs in the ER and that LVPs bud off from the ER in COPII vesicles and traffic through the Golgi secretory pathway.

MATERIALS AND METHODS

Cell culture and HCV infection. Huh7-derived Huh7.5.1 human hepatoma cells were cultured in Dulbecco's modified Eagle's medium supplemented with 10% fetal bovine serum, 100 U/ml penicillin, and 100 μg/ml streptomycin (Invitrogen, Carlsbad, CA) at 37°C in 5% CO_2. The HCVcc JFH D183 mutant of genotype 2a used in this study was propagated and prepared as described previously (32). JFH D183 is a chronic-phase virus that was collected on day 183 after transfection of the JFH genome and harbors a G451R mutation in the E2 region responsible for rapid viral expansion kinetics and high infectious titers (42). Both Huh7.5.1 cells and JFH D183 virus are generous gifts from F. Chisari (The Scripps Institute, La Jolla, CA). Huh7.5.1 cells were infected at an MOI of 1 for all experiments in this study.

Cytosol preparation and iodixanol gradient fractionation. At 72 h postinfection, JFH D183-infected Huh7.5.1 cells were scraped into ice-cold phosphate-buffered saline (PBS) and centrifuged at 2,000 rpm for 3 min to pellet the cells. The cell pellet was resuspended in isotonic medium (250 mM sucrose, 25 mM KCl, 10 mM HEPES [pH 7.2], 1 mM EGTA, and protease inhibitors) and subjected to nondenaturing cell lysis in a nitrogen gas-pressurized pressure bomb at 1,000 lb/in^2 for 25 min. This nondenaturing cell lysis method was adopted to retain intracellular transport vesicle (COPII vesicle) integrity. The cell lysate obtained was subjected to centrifugation at 1,000 rpm for 10 min to obtain the postnuclear supernatant, which was then subjected to centrifugation at 12,000 rpm for 20 min to obtain the postmitochondrial supernatant (PMS). The PMS was subsequently ultracentrifuged at 100,000 $\times$ *g* for 1 h to obtain the cytosol fraction. The cytosol was concentrated 10- to 20-fold by using 3-kDa-cutoff Amicon filters. The concentrated cytosol was overlaid on a 6 to 30% continuous iodixanol gradient and ultracentrifuged at 100,000 $\times$ g for 6 h. The resolved gradient was fractionated into 20 500-μl fractions from top to bottom by using an ISCO density gradient fractionator.

Immunoprecipitation of COPII vesicles. The 500-μl cytosol fractions obtained after density gradient fractionation were diluted in equal volumes of isotonic buffer and subjected to preclearing with 50 μl of protein G-Sepharose beads (GE Healthcare) according to the manufacturer's protocols. The precleared cytosol was subjected to immunoprecipitation with mouse monoclonal anti-Sec31 antibody (Santa Cruz Biotech Inc.) overnight at 4°C under rotary agitation. Next, the immune complex was allowed to bind to

protein G-Sepharose by incubation of the cytosol-antibody conjugate mixture with 100 μl of beads at 4°C under rotary agitation for 4 h. The cytosol-antibody-bead mixture was washed three times in isotonic buffer to remove nonspecific binding. The immune complex bead mixture was resuspended in 400 μl isotonic buffer. One hundred microliters of the resuspension was used for RNA isolation and focus-forming unit assays, and the remaining 200 μl was used for Western blot analysis.

HCV titration. To determine the levels of HCV RNA, quantitative real-time PCR analysis using HCV-specific primers and probe was performed as described previously (53). The virus titer in the culture medium and cells was determined by an FFU assay as described previously (20, 32). Briefly, log fold dilutions of the infectious cell culture medium were used to infect naive Huh7.5.1 cells. At 72 h postinfection, the cells were fixed and immunostained for the HCV E2 protein, and the number of HCV-positive foci was counted. For intracellular infectivity, the cell pellet was resuspended in complete medium and subjected to 3 to 4 cycles of freeze-thawing. The clarified cell lysate was used to perform FFU assays as described previously (20, 32).

Immunofluorescence. Cells grown on glass coverslips were fixed in 4% paraformaldehyde, washed, and then permeabilized with 50 μM digitonin. The cells were blocked in 1% bovine serum albumin (BSA)–PBS-Tween (PBST) for 1 h and then probed with primary antibody in blocking buffer overnight at 4°C. After 3 washes in PBS, the cells were stained with the respective Alexa Fluor secondary antibodies, raised in donkey (Invitrogen, Carlsbad, CA), for 1 h at room temperature. The antibody dilutions used were those recommended by the manufacturer. After the final wash, the coverslips were mounted onto ProLong Gold Antifade (Invitrogen, Carlsbad, CA). Images were visualized with an Olympus FluoView 1000 confocal microscope.

Immunoelectron microscopy. Huh7-derived Huh7.5.1 cells were infected at an MOI of 1 with the JFH D183 virus, and at 72 h postinfection, the cells were fixed in 4% paraformaldehyde in 0.1 M phosphate buffer (pH 7.4) overnight at 4°C. Fixed cells were washed with 0.15 M glycine-phosphate buffer, embedded in 10% gelatin-phosphate buffer, and infused with 2.3 M sucrose-phosphate buffer overnight at 4°C. One-cubic-millimeter cell blocks were mounted onto specimen holders and snap-frozen in liquid nitrogen. Ultracryomicrotomy was carried out at −100°C on a Leica Ultracut UCT with EM FCS cryoattachment (Leica, Bannockburn, IL) using a Diatome diamond knife (Diatome US, Hatfield, PA). Seventy- to ninety-nanometer frozen sections were picked up with a 1:1 mixture of 2.3 M sucrose and 2% methylcellulose (15 cP) as described previously by Liou et al. and Tokuyasu (54, 55) and transferred onto Formvar- and carbon-coated copper grids. Immunolabeling was performed by using a slight modification of the "Tokuyasu technique" (55). Briefly, grids were placed onto 2% gelatin at 37°C for 20 min and rinsed with 0.15 M glycine–PBS, and the sections were blocked by using 1% cold-water fish skin gelatin. Primary antibodies were diluted in 1% BSA–PBS. Incubation with primary antibodies for 2 h at room temperature was followed by incubation with the respective secondary antibodies (12- or 18-nm gold-conjugated goat anti-mouse IgG at a 1:20 dilution, 12- or 18-nm gold-conjugated goat anti-rabbit IgG at a 1:15 dilution, 6-nm gold-conjugated goat anti-human at a 1:10 dilution, 6-nm gold-conjugated donkey anti-mouse at a 1:15 dilution, and 18-nm gold-conjugated donkey anti-goat at a 1:15 dilution) from Jackson ImmunoResearch (West Grove, PA) diluted in 1% BSA–PBS at room temperature for 45 min. Grids were viewed by using a JEOL 1200EX II transmission electron microscope (JEOL, Peabody, MA) and photographed by using a Gatan digital camera (Gatan, Pleasanton, CA).

siRNA transfection and HCV infection. siRNA pools used in this study were siGENOME SMARTpool for CideB, KLHL12, and sortilin and nontargeting siRNA 1 (Dharmacon). Huh7.5.1 cells were infected with the JFH D183 virus at an MOI of 1. At 24 h postinfection, the cells were transfected with siRNA (30 nM) by using Lipofectamine RNAiMax transfection reagent (Invitrogen) according to the manufacturer's instructions. At 72 h posttransfection, the cell culture supernatant and cells were collected to determine extracellular and intracellular HCV titers and HCV RNA levels as described previously (56).

Antibodies. The following primary antibodies were used in this study: mouse monoclonal anti-Sec31A, anti-Sec13, anti-Sec24, anti-Sec22b, and anti-CideB; antitransferrin and anticalnexin (Santa Cruz Biotech); rabbit polyclonal anti-Sec31A and anti-GAPDH (Santa Cruz Biotech); rabbit polyclonal anti-Sec23b, anti-Sec24a, anti-ApoB, antisortilin, and anti-mannosidase II antibodies (Abcam); rabbit monoclonal anti-ApoE (Abcam); rabbit monoclonal anti-ApoE, rabbit polyclonal antialbumin, rabbit polyclonal anti-β-actin, and mouse monoclonal anti-KLHL12 (Cell Signaling Tech); goat polyclonal anti-ApoB (Chemicon Inc.); Rabbit polyclonal anti-TGN46 (Sigma); mouse monoclonal anti-dsRNA J2 antibody (Scicons, Hungary); mouse monoclonal anti-HCV core (Thermo Scientific); and human monoclonal anti-HCV E2 antibody AR3A (57) (a gift from Mansun Law, The Scripps Research Institute, CA). The secondary antibodies used for immunofluorescence were donkey anti-mouse, donkey anti-rabbit, and goat anti-human antibodies labeled with Alexa Fluor 488, 594, or 647 (Invitrogen, CA). The gold particle-conjugated goat anti-mouse, goat anti-rabbit, and goat anti-human antibodies were obtained from Jackson Laboratories.

ACKNOWLEDGMENTS

This work is supported by NIH grants to A.S. (AI085087 and DK077704).

We thank Francis Chisari (The Scripps Research Institute, La Jolla, CA) for providing the HCV JFH strain and Mansun Law (The Scripps Research Institute, La Jolla, CA) for providing the HCV E2 antibody. Electron microscopy was carried out at the University of California, San Diego, EM core facility. We also thank Marilyn Farquhar for immunoelectron microscopy analysis.

REFERENCES

1. Lavanchy D. 2011. Evolving epidemiology of hepatitis C virus. Clin Microbiol Infect 17:107–115. https://doi.org/10.1111/j.1469-0691.2010.03432.x.
2. Hoofnagle JH. 2002. Course and outcome of hepatitis C. Hepatology 36:S21–S29. https://doi.org/10.1002/hep.1840360704.
3. Mackenzie JM, Westaway EG. 2001. Assembly and maturation of the flavivirus Kunjin virus appear to occur in the rough endoplasmic reticulum and along the secretory pathway, respectively. J Virol 75:10787–10799. https://doi.org/10.1128/JVI.75.22.10787-10799.2001.
4. Mettenleiter TC. 2002. Herpesvirus assembly and egress. J Virol 76:1537–1547. https://doi.org/10.1128/JVI.76.4.1537-1547.2002.
5. Krijnse-Locker J, Ericsson M, Rottier PJ, Griffiths G. 1994. Characterization of the budding compartment of mouse hepatitis virus: evidence that transport from the RER to the Golgi complex requires only one vesicular transport step. J Cell Biol 124:55–70. https://doi.org/10.1083/jcb.124.1.55.
6. Johnson DC, Baines JD. 2011. Herpesviruses remodel host membranes for virus egress. Nat Rev Microbiol 9:382–394. https://doi.org/10.1038/nrmicro2559.
7. Salanueva IJ, Novoa RR, Cabezas P, Lopez-Iglesias C, Carrascosa JL, Elliott RM, Risco C. 2003. Polymorphism and structural maturation of bunyamwera virus in Golgi and post-Golgi compartments. J Virol 77:1368–1381. https://doi.org/10.1128/JVI.77.2.1368-1381.2003.
8. Lopez T, Camacho M, Zayas M, Najera R, Sanchez R, Arias CF, Lopez S. 2005. Silencing the morphogenesis of rotavirus. J Virol 79:184–192. https://doi.org/10.1128/JVI.79.1.184-192.2005.
9. Andre P, Komurian-Pradel F, Deforges S, Perret M, Berland JL, Sodoyer M, Pol S, Brechot C, Paranhos-Baccala G, Lotteau V. 2002. Characterization of low- and very-low-density hepatitis C virus RNA-containing particles. J Virol 76:6919–6928. https://doi.org/10.1128/JVI.76.14.6919-6928.2002.
10. Bartenschlager R, Penin F, Lohmann V, Andre P. 2011. Assembly of infectious hepatitis C virus particles. Trends Microbiol 19:95–103. https://doi.org/10.1016/j.tim.2010.11.005.
11. Nielsen SU, Bassendine MF, Burt AD, Martin C, Pumeechockchai W, Toms GL. 2006. Association between hepatitis C virus and very-low-density lipoprotein (VLDL)/LDL analyzed in iodixanol density gradients. J Virol 80:2418–2428. https://doi.org/10.1128/JVI.80.5.2418-2428.2006.
12. Nielsen SU, Bassendine MF, Martin C, Lowther D, Purcell PJ, King BJ, Neely D, Toms GL. 2008. Characterization of hepatitis C RNA-containing particles from human liver by density and size. J Gen Virol 89:2507–2517. https://doi.org/10.1099/vir.0.2008/000083-0.
13. Gastaminza P, Dryden KA, Boyd B, Wood MR, Law M, Yeager M, Chisari FV. 2010. Ultrastructural and biophysical characterization of hepatitis C virus particles produced in cell culture. J Virol 84:10999–11009. https://doi.org/10.1128/JVI.00526-10.
14. Hijikata M, Shimizu YK, Kato H, Iwamoto A, Shih JW, Alter HJ, Purcell RH, Yoshikura H. 1993. Equilibrium centrifugation studies of hepatitis C virus: evidence for circulating immune complexes. J Virol 67:1953–1958.
15. Kanto T, Hayashi N, Takehara T, Hagiwara H, Mita E, Naito M, Kasahara A, Fusamoto H, Kamada T. 1994. Buoyant density of hepatitis C virus recovered from infected hosts: two different features in sucrose equilibrium density-gradient centrifugation related to degree of liver inflammation. Hepatology 19:296–302. https://doi.org/10.1002/hep.1840190206.
16. Aizaki H, Morikawa K, Fukasawa M, Hara H, Inoue Y, Tani H, Saito K, Nishijima M, Hanada K, Matsuura Y, Lai MM, Miyamura T, Wakita T, Suzuki T. 2008. Critical role of virion-associated cholesterol and sphingolipid in hepatitis C virus infection. J Virol 82:5715–5724. https://doi.org/10.1128/JVI.02530-07.
17. Maillard P, Walic M, Meuleman P, Roohvand F, Huby T, Le Goff W, Leroux-Roels G, Pecheur EI, Budkowska A. 2011. Lipoprotein lipase inhibits hepatitis C virus (HCV) infection by blocking virus cell entry. PLoS One 6:e26637. https://doi.org/10.1371/journal.pone.0026637.
18. Catanese MT, Uryu K, Kopp M, Edwards TJ, Andrus L, Rice WJ, Silvestry M, Kuhn RJ, Rice CM. 2013. Ultrastructural analysis of hepatitis C virus particles. Proc Natl Acad Sci U S A 110:9505–9510. https://doi.org/10.1073/pnas.1307527110.
19. Merz A, Long G, Hiet MS, Brugger B, Chlanda P, Andre P, Wieland F, Krijnse-Locker J, Bartenschlager R. 2011. Biochemical and morphological properties of hepatitis C virus particles and determination of their lipidome. J Biol Chem 286:3018–3032. https://doi.org/10.1074/jbc.M110.175018.
20. Gastaminza P, Cheng G, Wieland S, Zhong J, Liao W, Chisari FV. 2008. Cellular determinants of hepatitis C virus assembly, maturation, degradation, and secretion. J Virol 82:2120–2129. https://doi.org/10.1128/JVI.02053-07.
21. Huang H, Sun F, Owen DM, Li W, Chen Y, Gale M, Jr, Ye J. 2007. Hepatitis C virus production by human hepatocytes dependent on assembly and secretion of very low-density lipoproteins. Proc Natl Acad Sci U S A 104:5848–5853. https://doi.org/10.1073/pnas.0700760104.
22. Jiang J, Luo G. 2009. Apolipoprotein E but not B is required for the formation of infectious hepatitis C virus particles. J Virol 83:12680–12691. https://doi.org/10.1128/JVI.01476-09.
23. Shelness GS, Sellers JA. 2001. Very-low-density lipoprotein assembly and secretion. Curr Opin Lipidol 12:151–157. https://doi.org/10.1097/00041433-200104000-00008.
24. Beilstein F, Lemasson M, Pene V, Rainteau D, Demignot S, Rosenberg AR. 31 August 2016. Lysophosphatidylcholine acyltransferase 1 is down-regulated by hepatitis C virus: impact on production of lipo-viro-particles. Gut https://doi.org/10.1136/gutjnl-2016-311508.
25. Vieyres G, Welsch K, Gerold G, Gentzsch J, Kahl S, Vondran FW, Kaderali L, Pietschmann T. 2016. ABHD5/CGI-58, the Chanarin-Dorfman syndrome protein, mobilises lipid stores for hepatitis C virus production. PLoS Pathog 12:e1005568. https://doi.org/10.1371/journal.ppat.1005568.
26. Cai H, Yao W, Li L, Li X, Hu L, Mai R, Peng T. 2016. Cell-death-inducing DFFA-like effector B contributes to the assembly of hepatitis C virus (HCV) particles and interacts with HCV NS5A. Sci Rep 6:27778. https://doi.org/10.1038/srep27778.
27. Lee JY, Acosta EG, Stoeck IK, Long G, Hiet MS, Mueller B, Fackler OT, Kallis S, Bartenschlager R. 2014. Apolipoprotein E likely contributes to a maturation step of infectious hepatitis C virus particles and interacts with viral envelope glycoproteins. J Virol 88:12422–12437. https://doi.org/10.1128/JVI.01660-14.
28. Mankouri J, Walter C, Stewart H, Bentham M, Park WS, Heo WD, Fukuda M, Griffin S, Harris M. 2016. Release of infectious hepatitis C virus from Huh7 cells occurs via a trans-Golgi network-to-endosome pathway independent of very-low-density lipoprotein secretion. J Virol 90:7159–7170. https://doi.org/10.1128/JVI.00826-16.
29. Gondar V, Molina-Jimenez F, Hishiki T, Garcia-Buey L, Koutsoudakis G, Shimotohno K, Benedicto I, Majano PL. 2015. Apolipoprotein E, but not apolipoprotein B, is essential for efficient cell-to-cell transmission of hepatitis C virus. J Virol 89:9962–9973. https://doi.org/10.1128/JVI.00577-15.
30. Hueging K, Doepke M, Vieyres G, Bankwitz D, Frentzen A, Doerrbecker J, Gumz F, Haid S, Wolk B, Kaderali L, Pietschmann T. 2014. Apolipoprotein E codetermines tissue tropism of hepatitis C virus and is crucial for viral cell-to-cell transmission by contributing to a postenvelopment step of assembly. J Virol 88:1433–1446. https://doi.org/10.1128/JVI.01815-13.
31. Coller KE, Heaton NS, Berger KL, Cooper JD, Saunders JL, Randall G. 2012. Molecular determinants and dynamics of hepatitis C virus secretion. PLoS Pathog 8:e1002466. https://doi.org/10.1371/journal.ppat.1002466.
32. Amako Y, Syed GH, Siddiqui A. 2011. Protein kinase D negatively regulates hepatitis C virus secretion through phosphorylation of oxysterol-binding protein and ceramide transfer protein. J Biol Chem 286:11265–11274. https://doi.org/10.1074/jbc.M110.182097.
33. Bishe B, Syed GH, Field SJ, Siddiqui A. 2012. Role of phosphatidylinositol 4-phosphate (PI4P) and its binding protein GOLPH3 in hepatitis C virus secretion. J Biol Chem 287:27637–27647. https://doi.org/10.1074/jbc.M112.346569.
34. Bayer K, Banning C, Bruss V, Wiltzer-Bach L, Schindler M. 2016. Hepatitis C virus is released via a noncanonical secretory route. J Virol 90:10558–10573. https://doi.org/10.1128/JVI.01615-16.
35. Benedicto I, Gondar V, Molina-Jimenez F, Garcia-Buey L, Lopez-Cabrera M, Gastaminza P, Majano PL. 2015. Clathrin mediates infectious hepatitis C virus particle egress. J Virol 89:4180–4190. https://doi.org/10.1128/JVI.03620-14.
36. Corless L, Crump CM, Griffin SD, Harris M. 2010. Vps4 and the ESCRT-III complex are required for the release of infectious hepatitis C virus particles. J Gen Virol 91:362–372. https://doi.org/10.1099/vir.0.017285-0.
37. Elgner F, Ren H, Medvedev R, Ploen D, Himmelsbach K, Boller K, Hildt E. 2016. The intracellular cholesterol transport inhibitor U18666A

inhibits the exosome-dependent release of mature hepatitis C virus. J Virol 90:11181–11196. https://doi.org/10.1128/JVI.01053-16.
38. Gomez-Navarro N, Miller E. 2016. Protein sorting at the ER-Golgi interface. J Cell Biol 215:769–778.
39. Malhotra V, Erlmann P. 2011. Protein export at the ER: loading big collagens into COPII carriers. EMBO J 30:3475–3480. https://doi.org/10.1038/emboj.2011.255.
40. Icard V, Diaz O, Scholtes C, Perrin-Cocon L, Ramiere C, Bartenschlager R, Penin F, Lotteau V, Andre P. 2009. Secretion of hepatitis C virus envelope glycoproteins depends on assembly of apolipoprotein B positive lipoproteins. PLoS One 4:e4233. https://doi.org/10.1371/journal.pone.0004233.
41. Siddiqi SA. 2008. VLDL exits from the endoplasmic reticulum in a specialized vesicle, the VLDL transport vesicle, in rat primary hepatocytes. Biochem J 413:333–342. https://doi.org/10.1042/BJ20071469.
42. Zhong J, Gastaminza P, Chung J, Stamataki Z, Isogawa M, Cheng G, McKeating JA, Chisari FV. 2006. Persistent hepatitis C virus infection in vitro: coevolution of virus and host. J Virol 80:11082–11093. https://doi.org/10.1128/JVI.01307-06.
43. Vieyres G, Dubuisson J, Pietschmann T. 2014. Incorporation of hepatitis C virus E1 and E2 glycoproteins: the keystones on a peculiar virion. Viruses 6:1149–1187. https://doi.org/10.3390/v6031149.
44. Butkinaree C, Guo L, Ramkhelawon B, Wanschel A, Brodsky JL, Moore KJ, Fisher EA. 2014. A regulator of secretory vesicle size, Kelch-like protein 12, facilitates the secretion of apolipoprotein B100 and very-low-density lipoproteins—brief report. Arterioscler Thromb Vasc Biol 34:251–254. https://doi.org/10.1161/ATVBAHA.113.302728.
45. Tiwari S, Siddiqi S, Siddiqi SA. 2013. CideB protein is required for the biogenesis of very low density lipoprotein (VLDL) transport vesicle. J Biol Chem 288:5157–5165. https://doi.org/10.1074/jbc.M112.434258.
46. Strong A, Ding Q, Edmondson AC, Millar JS, Sachs KV, Li X, Kumaravel A, Wang MY, Ai D, Guo L, Alexander ET, Nguyen D, Lund-Katz S, Phillips MC, Morales CR, Tall AR, Kathiresan S, Fisher EA, Musunuru K, Rader DJ. 2012. Hepatic sortilin regulates both apolipoprotein B secretion and LDL catabolism. J Clin Invest 122:2807–2816. https://doi.org/10.1172/JCI63563.
47. Sheridan DA, Hajarizadeh B, Fenwick FI, Matthews GV, Applegate T, Douglas M, Neely D, Askew B, Dore GJ, Lloyd AR, George J, Bassendine MF, Grebely J. 2016. Maximum levels of hepatitis C virus lipoviral particles are associated with early and persistent infection. Liver Int 36:1774–1782. https://doi.org/10.1111/liv.13176.
48. Lussignol M, Kopp M, Molloy K, Vizcay-Barrena G, Fleck RA, Dorner M, Bell KL, Chait BT, Rice CM, Catanese MT. 2016. Proteomics of HCV virions reveals an essential role for the nucleoporin Nup98 in virus morphogenesis. Proc Natl Acad Sci U S A 113:2484–2489. https://doi.org/10.1073/pnas.1518934113.
49. Barouch-Bentov R, Neveu G, Xiao F, Beer M, Bekerman E, Schor S, Campbell J, Boonyaratanakornkit J, Lindenbach B, Lu A, Jacob Y, Einav S. 2016. Hepatitis C virus proteins interact with the endosomal sorting complex required for transport (ESCRT) machinery via ubiquitination to facilitate viral envelopment. mBio 7:e01456-16. https://doi.org/10.1128/mBio.01456-16.
50. Boyer A, Dumans A, Beaumont E, Etienne L, Roingeard P, Meunier JC. 2014. The association of hepatitis C virus glycoproteins with apolipoproteins E and B early in assembly is conserved in lipoviral particles. J Biol Chem 289:18904–18913. https://doi.org/10.1074/jbc.M113.538256.
51. Yang Z, Wang X, Chi X, Zhao F, Guo J, Ma P, Zhong J, Niu J, Pan X, Long G. 2016. Neglected but important role of apolipoprotein E exchange in hepatitis C virus infection. J Virol 90:9632–9643. https://doi.org/10.1128/JVI.01353-16.
52. Strong A, Patel K, Rader DJ. 2014. Sortilin and lipoprotein metabolism: making sense out of complexity. Curr Opin Lipidol 25:350–357. https://doi.org/10.1097/MOL.0000000000000110.
53. Takeuchi T, Katsume A, Tanaka T, Abe A, Inoue K, Tsukiyama-Kohara K, Kawaguchi R, Tanaka S, Kohara M. 1999. Real-time detection system for quantification of hepatitis C virus genome. Gastroenterology 116:636–642. https://doi.org/10.1016/S0016-5085(99)70185-X.
54. Liou W, Geuze HJ, Slot JW. 1996. Improving structural integrity of cryosections for immunogold labeling. Histochem Cell Biol 106:41–58. https://doi.org/10.1007/BF02473201.
55. Tokuyasu KT. 1980. Immunochemistry on ultrathin frozen sections. Histochem J 12:381–403. https://doi.org/10.1007/BF01011956.
56. Syed GH, Siddiqui A. 2011. Effects of hypolipidemic agent nordihydroguaiaretic acid on lipid droplets and hepatitis C virus. Hepatology 54:1936–1946. https://doi.org/10.1002/hep.24619.
57. Giang E, Dorner M, Prentoe JC, Dreux M, Evans MJ, Bukh J, Rice CM, Ploss A, Burton DR, Law M. 2012. Human broadly neutralizing antibodies to the envelope glycoprotein complex of hepatitis C virus. Proc Natl Acad Sci U S A 109:6205–6210. https://doi.org/10.1073/pnas.1114927109.